Nuclear Engineering and Technology 48 (2016) 660–672

Available online at ScienceDirect

Nuclear Engineering and Technology

journal homepage: www.elsevier.com/locate/net

Original Article

Steady- and Transient-State Analyses of Fully Ceramic Microencapsulated Fuel with Randomly Dispersed Tristructural Isotropic Particles via Two-Temperature Homogenized Model—II: Applications by Coupling with COREDAX

Yoonhee Lee [1], *Bumhee Cho* [2], *and Nam Zin Cho* [*]

Department of Nuclear and Quantum Engineering, Korea Advanced Institute of Science and Technology, 291 Daehak-ro, Yuseong-gu, Daejeon 34141, Republic of Korea

ARTICLE INFO

Article history:
Received 28 December 2015
Received in revised form
27 January 2016
Accepted 9 February 2016
Available online 3 March 2016

Keywords:
Doppler Temperature Feedback
Fine Lattice Stochastic Structure
Fully Ceramic Microencapsulated Fuel
Harmonic- and Volumetric-Average Thermal Conductivities
Reactor Physics Asia 2015
Two-Temperature Homogenized Model

ABSTRACT

In Part I of this paper, the two-temperature homogenized model for the fully ceramic microencapsulated fuel, in which tristructural isotropic particles are randomly dispersed in a fine lattice stochastic structure, was discussed. In this model, the fuel-kernel and silicon carbide matrix temperatures are distinguished. Moreover, the obtained temperature profiles are more realistic than those obtained using other models. Using the temperature-dependent thermal conductivities of uranium nitride and the silicon carbide matrix, temperature-dependent homogenized parameters were obtained. In Part II of the paper, coupled with the COREDAX code, a reactor core loaded by fully ceramic microencapsulated fuel in which tristructural isotropic particles are randomly dispersed in the fine lattice stochastic structure is analyzed via a two-temperature homogenized model at steady and transient states. The results are compared with those from harmonic- and volumetric-average thermal conductivity models; i.e., we compare k_{eff} eigenvalues, power distributions, and temperature profiles in the hottest single channel at a steady state. At transient states, we compare total power, average energy deposition, and maximum temperatures in the hottest single channel obtained by the different thermal analysis models. The different thermal analysis models and the availability of fuel-kernel temperatures in the two-temperature homogenized model for Doppler temperature feedback lead to significant differences.

* *Corresponding author.*
E-mail address: nzcho@kaist.ac.kr (N.Z. Cho).
[1] Present address: Korea Institute of Nuclear Safety, 62 Gwahak-ro, Yuseong-gu, Daejeon 34142, Republic of Korea.
[2] Present address: Standard Energy, 32-16 Techno 7-ro, Yuseong-gu, Daejeon 34029, Republic of Korea.

http://dx.doi.org/10.1016/j.net.2016.02.006

1. Introduction

This is the second part of a two-part paper. Part I [1] of the paper describes the two-temperature homogenized model and calculation method of temperature-dependent homogenized parameters for the fully ceramic microencapsulated (FCM) fuel element in which tristructural isotropic (TRISO) particles are based on a uranium nitride kernel and the particles are randomly dispersed in the fine lattice stochastic structure [2]. In Part II, coupled with a reactor analysis module in COREDAX based on the analytic function expansion nodal method for the neutron diffusion model [3], a reactor core loaded by FCM fuels is analyzed via the two-temperature homogenized model in steady- and transient-state scenarios. The results are compared with those of the harmonic- and volumetric-average thermal conductivity models. In the analyses, thermophysical properties of the FCM pellet, including the homogenized parameters in the two-temperature homogenized model and cross sections of the neutron diffusion model, are considered to be temperature dependent. In Part I, the temperature-dependent homogenized parameters are generated based on the temperature-dependent thermal properties of uranium nitride [4,5], which is now being focused on as a material for fuel kernels in the FCM and the temperature-dependent thermal properties of the silicon carbide (SiC) matrix [6,7]. In Part II, the temperature-dependent two-group cross sections in the neutron diffusion model are generated by a lattice physics calculation using the Serpent code [8] with temperature-dependent, continuous-energy cross-section libraries processed by the NJOY code [9]. For temperature feedback on the cross sections in the neutron diffusion model, the effective temperatures of the FCM fuels are calculated by preserving the reactivity from the temperature profiles for various packing fractions. In the analyses, the effective temperatures of the fuel kernels, Doppler temperatures, effective temperatures of the SiC matrix, helium gap, SiC cladding, and the coolant at each axial plane are considered. For the harmonic- and volumetric-average thermal conductivity models, since they cannot provide fuel-kernel temperatures explicitly, the effective temperatures of the FCM pellet are used as the Doppler temperatures.

In the steady-state analyses, we compare the following: (1) k_{eff} eigenvalues; (2) power distributions; and (3) temperature profiles in the hottest single channel. In the transient-state analyses, we consider a reactivity-initiated accident induced by slow and fast control rod withdrawal as transient scenarios. In addition, we compare the following: (1) total power; (2i) average energy deposition, which is the key regulatory quantity for a reactivity-initiated accident; and (3) the maximum temperatures in the hottest single channel. The differences in the results originate from different thermophysical properties of the FCM pellets used in different thermal analysis models and the availability of fuel-kernel temperatures. Therefore, we focus on those aspects for comparison.

This paper is organized as follows. Section 2 provides a brief description of coupling of the thermal analysis models and COREDAX. In Section 3, numerical results are provided to compare the thermal analysis models in steady- and transient-state analyses. Finally, discussions and conclusions are provided in Section 4.

2. Coupling of thermal analysis models with COREDAX

2.1. Generation of temperature-dependent two-group cross sections for neutron diffusion model

The reactor analysis code, COREDAX, which is based on the analytic function expansion nodal method for the neutron diffusion model, is coupled with the thermal analysis models explained in Sections 2 and 3 in Part I of this paper [1]. Temperature-dependent two-group cross sections in the neutron diffusion model are generated by lattice physics calculations using the Serpent code [8] with temperature-dependent continuous-energy cross-section libraries processed by the NJOY code [9]. In the lattice physics calculation, the geometry is derived from a Westinghouse 17 × 17 assembly. The assembly configuration used in this study is shown in Table 1. Modeling of the assembly used in the Serpent code is illustrated in Fig. 1. In the Serpent calculation, TRISO particles are explicitly modeled and distributed in the fine lattice stochastic structure, as in the HEATON modeling shown in Fig. 1.

2.2. Effective temperatures of the FCM fuel and temperature feedback on COREDAX

In the reactor, there is a fuel temperature distribution that must be taken into account while calculating the reactivity effect. It can be taken into account in the neutron diffusion model through the changes in cross sections, which are space dependent since the temperature changes are also space dependent. Studies of the effect of temperature variation within an actual fuel rod indicate that the use of an effective temperature yields adequate accuracy [10]. Therefore, the effective temperature of the FCM fuel should be calculated so that the reactivity from the temperature profiles is preserved.

In this study, the Serpent code is used to calculate the effective temperatures with the temperature-dependent continuous energy cross-section libraries processed by the NJOY code [9]. For reference calculation of the multiplication factor (k_{inf}), a single rod of the FCM fuel with a packing fraction of 0.388 is divided into four rings so that the temperature

Table 1 – Assembly configuration for lattice physics calculation.

Parameters		Values
Number of fuel rods		264
Number of guide tubes		24
Radius of guide tube (inner, outer) (cm)		1.123, 1.204
Pellet radius		0.4095
Gap	Radius (cm)	0.418
	Material	He
Cladding	Radius (cm)	0.475
	Material	SiC
Fuel pitch (cm)		1.26

SiC, silicon carbide.

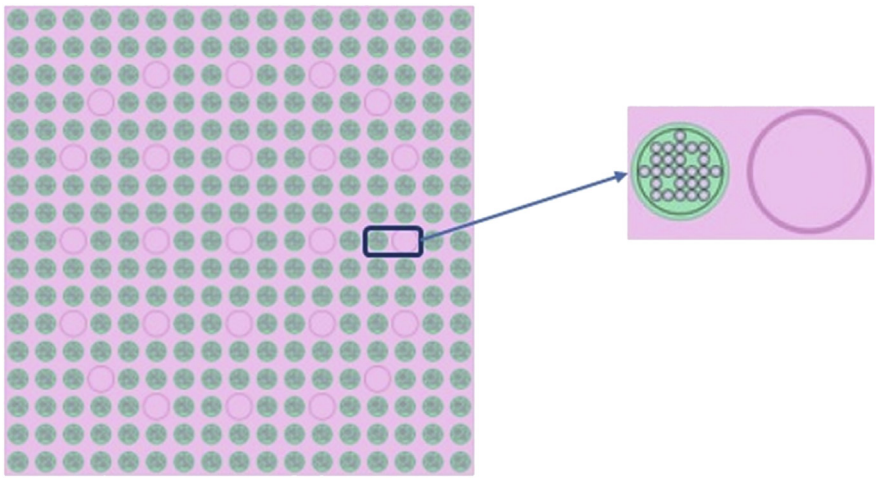

Fig. 1 – Illustration of an assembly in the Serpent code.

changes within each ring are less than ~50 K. In this case, it is sufficiently accurate to consider cross sections within each ring as temperature independent in the Monte Carlo calculation. The average temperatures of each ring are calculated via detailed temperature profiles of the FCM fuel element. Configuration of the reference calculations is shown in Fig. 2 and Table 2.

The volume-weighted average temperature of the configuration shown in Fig. 2 and Table 2 is 856.2 K and k_{inf} is 1.447150, which is calculated with 100,000 histories and 1,200 total cycles (200 inactive cycles).

Then, k_{inf} calculations are performed for the FCM fuel pin shown in Fig. 3 and Table 3, but using homogeneous temperature libraries of 947 K, 893 K, and 765 K. Results of k_{inf} are provided in Table 4.

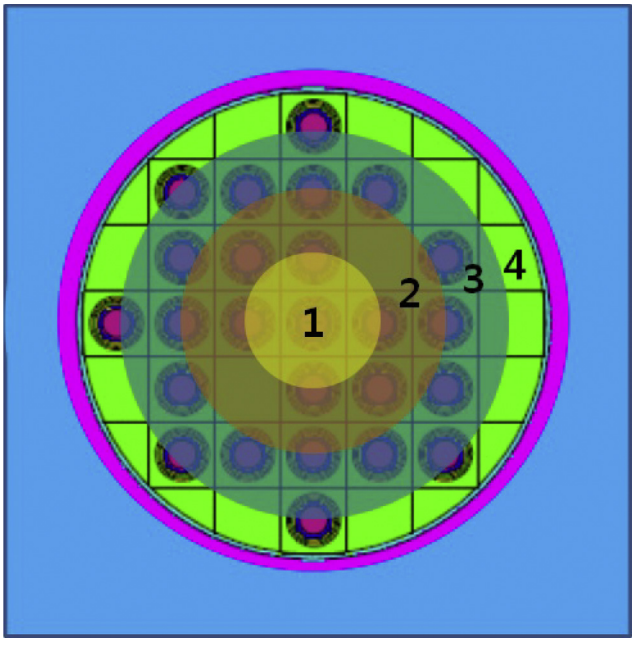

Fig. 2 – Illustration of a single FCM fuel pin for reference reactivity calculation. FCM, fully ceramic microencapsulated.

The reference k_{inf} is between the k_{inf} values of 893 K and 947 K. Interpolating k_{inf} between 893 K and 947 K yields the following:

$$k_{inf}(T) = -1.38889 \times 10^{-5} T + 1.459582778 \quad (893\,K \leq T \leq 947K) \tag{1}$$

Then, using the reference k_{inf}, the effective temperature is calculated as follows:

$$\overline{T}_{eff} = \frac{1.45982778 - k_{inf}(ref)}{1.38889 \times 10^{-5}} = 895.2 \tag{2}$$

Using Eq. (2) and the volume-weighted average temperature, the following relationship is obtained:

$$\overline{T}_{eff} = \alpha T_{avg} \tag{3}$$

If the procedures explained in this section are performed for various packing fractions, packing fraction-dependent α values are obtained, as shown in Fig. 4. The α values for various enrichments of the conventional UO_2 fuel are also presented in Fig. 4.

As shown in Fig. 4, the value of α decreases as the packing fraction increases. This result is caused by the mean free paths for the various packing fractions, as shown in Fig. 5. As the packing fraction increases, the mean free path decreases; that is, thermal neutrons, having energy less than 1 eV,

Table 2 – Configuration of the single FCM fuel pin for reference reactivity calculation.

Ring index	Radius (cm)	Average temperature (K)
1	0.117	971
2	0.234	947
3	0.351	893
4	0.4095	765

FCM, fully ceramic microencapsulated.

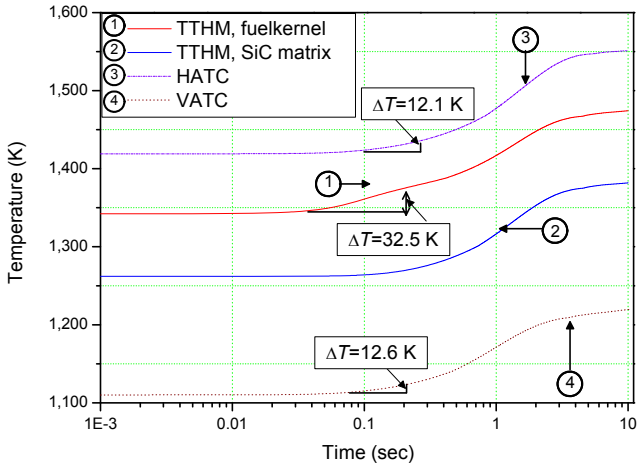

Fig. 3 – Maximum temperature changes during Scenario 1. HATC, harmonic-average thermal conductivity; SiC, silicon carbide; TTHM, two-temperature homogenized model; VATC, volumetric-average thermal conductivity.

migrate less distance. This means that fission reactions occur at positions nearer to the periphery of the fuel pin as the packing fraction increases.

The values of α for the FCM fuel are smaller than those of the conventional UO_2 fuel. The mean free paths of the two fuels are presented in Fig. 6.

As shown in Fig. 6, FCM fuel with a packing fraction of 0.38 shows shorter mean free paths than the conventional UO_2 fuel, with enrichment of 4.5 w/o. This means that fission reactions in the FCM fuel occur nearer to the periphery of the fuel than those in the conventional UO_2 fuel, which is consistent with the results shown in Fig. 4.

For the steady-state analysis, the assembly-averaged power distributions at each axial plane, obtained by neutron diffusion calculations of COREDAX, are divided by the number of fuel rods in the fuel assembly to obtain power distributions in the FCM fuel element. A single-channel thermal analysis is then performed via one of the three thermal analysis models: two-temperature homogenized model, or harmonic- or volumetric-average thermal conductivity models. Using the relationship between the average and effective temperatures shown in Eq. (3) for the appropriate packing fraction of the FCM fuel, and the effective temperatures of the fuel kernels (T_f) and those of the SiC matrix (T_m), helium gap (T_g), cladding

Table 3 – Thermophysical properties of the helium gap, SiC cladding, and water.

Parameters	Values
k_h (W/cm K)	0.0036
$(\rho c)_h$ (J/cm^3 K)	0.0104
k_c (W/cm K)	0.04
$(\rho c)_c$ (J/cm^3 K)	3.311
h (W/cm^{2}K)	4.223

SiC, silicon carbide.

Table 4 – The values of k_{inf} for FCM fuel pin using homogeneous temperature libraries.

Temperature (K)	k_{inf}
947	1.446430
893	1.447180
765	1.448550

(T_c), and coolant (T_b) at each axial plane, the two-group cross sections in the neutron diffusion model are then updated by the following equation [3]:

$$\sum_i(\overline{T}_f,\overline{T}_{mgc}) = \sum_i^r\left(T_f^r,T_{mgc}^r\right) + \left(\overline{T}_f - T_f^r\right)\left.\frac{\partial\Sigma_i^r}{\partial T_f}\right|_{\left(T_f^r,T_{mgc}^r\right)} + \left(\overline{T}_{mgc} - T_{mgc}^r\right)\left.\frac{\partial\Sigma_i^r}{\partial T_{mgc}}\right|_{\left(T_f^r,T_{mgc}^r\right)} \quad (4)$$

where

$\overline{T}_f$: effective temperature of the fuel kernels (T_f), Doppler temperature

$\overline{T}_{mgc}$: effective temperature of the SiC matrix (T_m), helium gap (T_g), cladding (T_c), and coolant (T_b)

Σ_i^r : cross section for reaction i at reference temperatures T_f^r and T_{mgc}^r.

For the harmonic- and volumetric-average thermal conductivity models, since they cannot provide fuel-kernel temperatures explicitly, the effective temperatures of the FCM pellet are used as the Doppler temperatures instead. Iterations are performed until the assembly-averaged power distributions converge.

For the transient-state analysis, the procedures of the steady-state analysis are performed at each time step. The calculational procedures in the steady- and transient-state analyses are summarized in Fig. 7.

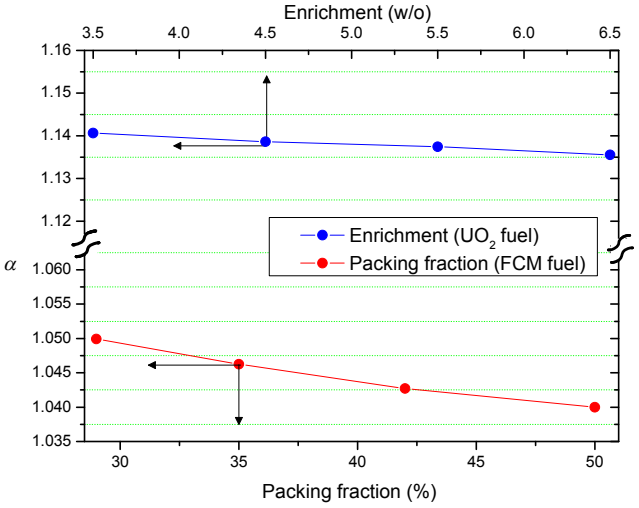

Fig. 4 – Packing fraction of the FCM fuel and enrichment of UO_2 versus α. FCM, fully ceramic microencapsulated.

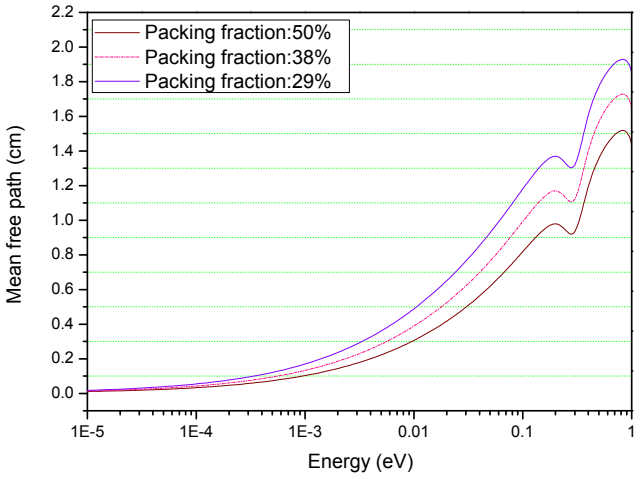

Fig. 5 – Packing fraction of the FCM fuel versus mean free path of thermal neutrons ($E < 1$ eV). FCM, fully ceramic microencapsulated.

3. Numerical results

3.1. *Steady-state analysis of the FCM fuel-loaded core and comparison of the thermal analysis models*

3.1.1. *Description of geometry information and computational conditions at steady state*

Reactor configurations used in the analysis are shown in Table 5 and Fig. 8. The configurations are derived from the Korean nuclear reactor Ulchin Unit I. The packing fraction of the pellet is 0.361, which is the same as that shown in the configuration of Figure 10 in Part I of this paper [1].

We use the homogenized parameters shown in Figures 12 and 13 in Part I of the paper [1]. The thermophysical properties of the helium gap, SiC cladding [11], and water used in the three models are listed in Table 3. Except for the coefficients listed in Table 6, all the thermophysical properties are considered to be temperature dependent.

For the three-dimensional neutron diffusion calculations, COREDAX is used. For a single-channel analysis in cylindrical geometry, a two-dimensional FDM in an R–Z geometry is used. Sweeping is used as a matrix equation solver in COREDAX. In the case of single-channel thermal analysis, BICGSTAB with a symmetric Gauss–Seidel preconditioner is used with a convergence criterion of 1.0E–7. The convergence criterion for the assembly-averaged power distributions is 1.0E–5. Detailed computational conditions are listed in Tables 7 and 8.

3.1.2. *Discussion of the results of steady-state analysis*

We perform a steady-state analysis to compare the three thermal analysis models: two-temperature homogenized model, and harmonic- and volumetric-average thermal conductivity explained in Sections 2 and 3 in Part I of this paper [1]. The k_{eff} eigenvalues and power distributions obtained from the COREDAX calculations are listed in Table 6 and Figs. 9 and 10.

As shown in Table 6, the k_{eff} eigenvalue differences between the two-temperature homogenized model and the harmonic-average thermal conductivity model is ~100 pcm. The difference between the two-temperature homogenized model and the volumetric-average thermal conductivity model is ~210 pcm. The differences are considerable; i.e., there is a difference of ~0.3 $ in reactivity, which may cause considerable differences in the critical boron concentration search and transient analysis. In case of power distributions, there is a difference of ~2% in power distribution obtained by the different thermal analysis models, as shown in Figs. 9 and 10.

The axial temperature profiles at the centerline of the FCM fuel element in assembly (6,5), which shows the largest power level among the assemblies in the reactor, are shown in Fig. 11.

At an elevation of z = 172.7 cm of assembly (6,5), the temperature difference between the two-temperature homogenized model and the harmonic-average thermal conductivity model is ~72.8 K. In addition, the difference between the two-temperature homogenized model and the volumetric-average thermal conductivity model is ~213.3 K. These differences are the maximum values along the fuel element in the assembly. For this elevation of the assembly, the radial temperature profiles of the three thermal analysis models are presented in Fig. 12. The maximum temperatures are listed in Table 9.

In the cladding, temperature differences between the three thermal analysis models are less than 5 K. However, in the FCM pellet, the differences become larger, approaching the center of the fuel element; i.e., the two-temperature homogenized model yields temperature profiles that are ~72.8 K lower than those of the harmonic-average thermal conductivity model and ~213.3 K higher than those of the volumetric-average thermal conductivity model at the center of the fuel element. These results are caused by the thermal conductivities of the SiC matrix, which is the major heat conduction medium in the two-temperature homogenized model. The thermal conductivities of the SiC matrix are ~1.37 times

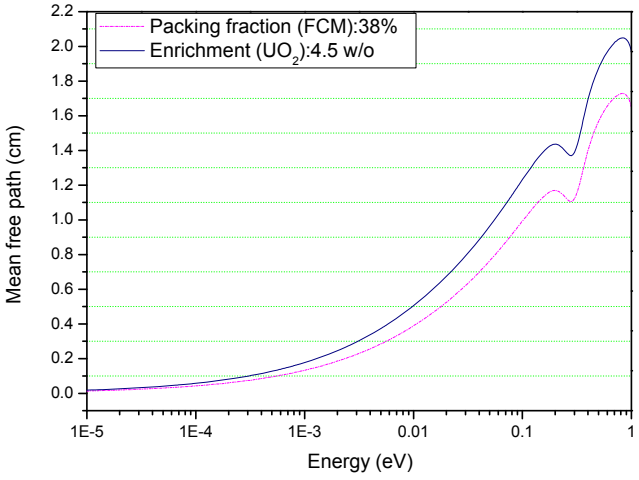

Fig. 6 – Packing fraction (FCM fuel) and enrichment (UO_2 fuel) versus mean free path. FCM, fully ceramic microencapsulated.

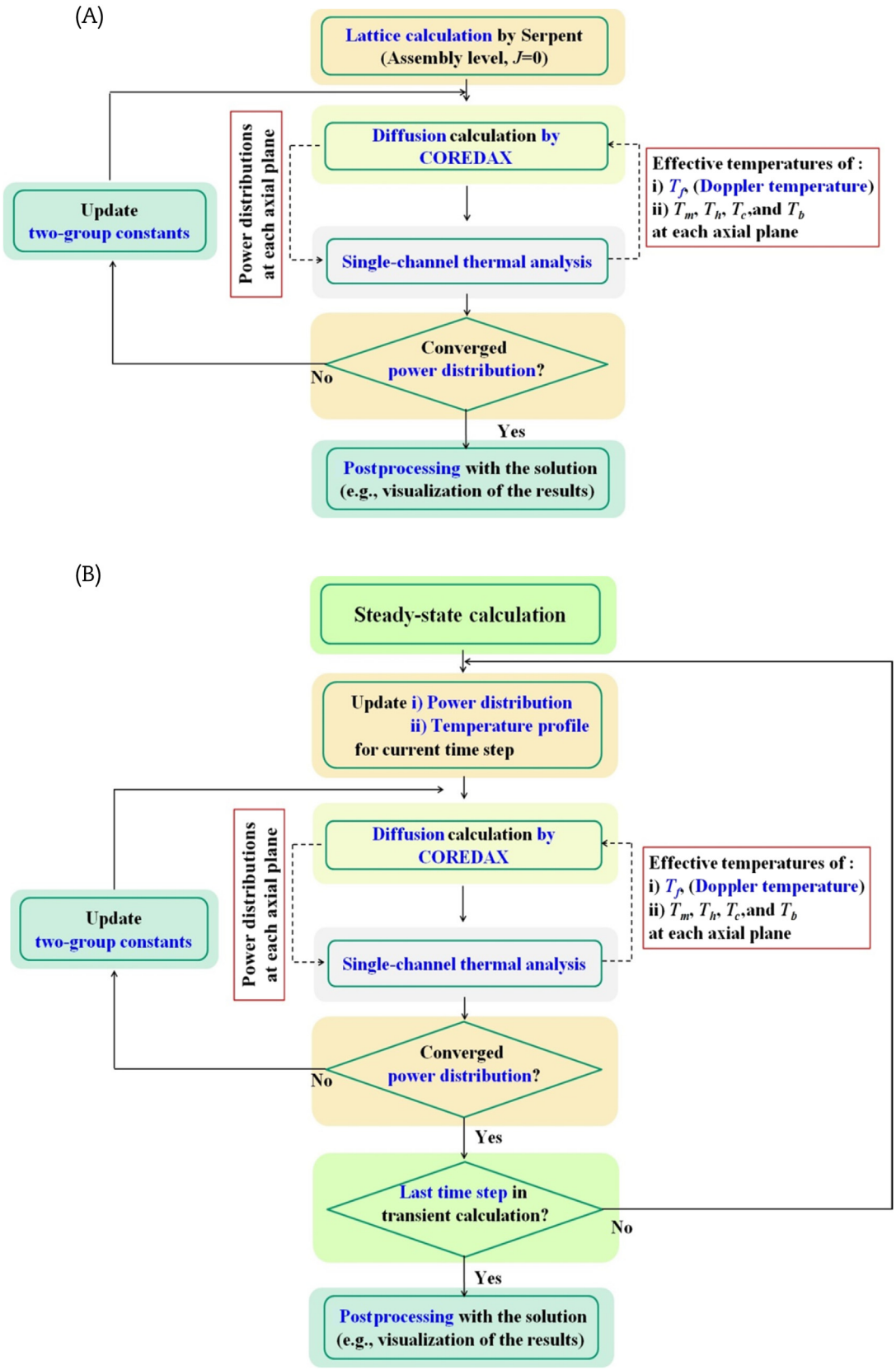

Fig. 7 – Calculational procedure of FCM fuel analysis coupled with the neutron diffusion model. (A) Steady-state calculational procedure. (B) Transient-state calculational procedure. FCM, fully ceramic microencapsulated.

Table 5 – Reactor configuration for steady-state analysis.

Parameters		Values
Power (MW)]		300.0 (1/8 core)
Enrichment of fuel (w/o)		19.7
Number of fuel assemblies		68
Number of fuel rods per assembly		264
Number of guide tubes per assembly		24
Active length (cm)]		386.08
Guide tube	Inner diameter (cm)	1.123
	Outer diameter (cm)	1.204
Coolant inlet temperature (K)		555.8

Table 6 – Comparison of the k_{eff} eigenvalues for the thermal analysis models.

	Thermal analysis model		
	TTHM	HATC	VATC
k_{eff}	1.112273	1.111280	1.114355
Difference[a] (pcm)	Reference	−99.26	208.21

HATC, harmonic-average thermal conductivity; TTHM, two-temperature homogenized model; VATC, volumetric-average thermal conductivity.
[a] Difference = HATC (or VATC) − TTHM.

Table 7 – Computational conditions of COREDAX for neutron diffusion calculations.

Parameters		Values
Cell size (x, y, z) (cm)	Fuel	21.5, 21.5, 20.32
	Reflector	21.5, 21.5, 20
Inner iteration method		Sweeping
Acceleration	Scheme	Coarse group rebalance
	Outer iteration number to start acceleration	30
	Number of iterations to update eigenvalue by acceleration	5
Source convergence criterion		1.0E−6

higher than those of the harmonic-average thermal conductivity and ~1.86 times lower than those of the volumetric-average thermal conductivity, as shown in Table 9.

3.2. *Transient-state analyses of the FCM fuel-loaded core and comparison of the thermal analysis models*

3.2.1. *Description of geometry information and computational conditions at transient state*

In this section, we consider two transient scenarios: (1) a reactivity-initiated accident in which control rods are withdrawn slowly from assembly (5,5) (which is denoted as Scenario 1 in the remainder of this chapter) and (2) a reactivity-initiated accident in which control rods are withdrawn rapidly from assembly (6,5) (which is denoted as Scenario 2 in the remainder of this chapter). The reactor configurations used in the transient analyses are shown in Fig. 13 and Table 10, and are similar to those used in the steady-state analysis, but with different locations of the control rod assemblies depending upon the scenario. Detailed scenarios of the transients and the corresponding results are presented in the following sections. If not specified in each section, the conditions such as coolant inlet temperature and total reactor power at the initial state are the same as those at the steady state. The homogenized parameters and thermophysical properties of the helium gap, cladding, and water used in the analyses are also the same as those at the steady state.

3.2.2. *Reactivity-initiated accident via slow control rod withdrawal*

In Scenario 1, initially, the control rods in assembly (5,5), in which the control rod worth is 865.8 pcm, are inserted at an elevation of z = 203.2 cm, as shown in Figs. 13 and 14, and Table 10, and they are withdrawn to an elevation of z = 406.08 cm with a speed of control rod movement of

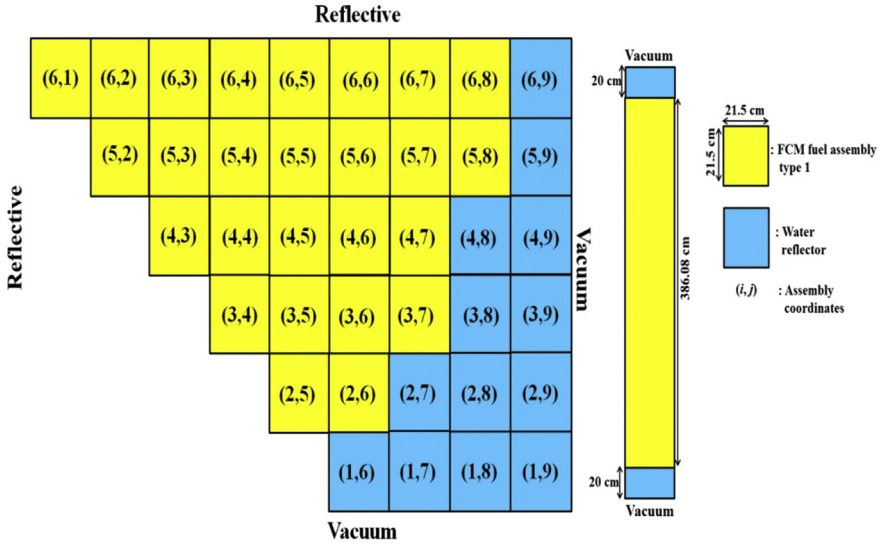

Fig. 8 – Radial and axial views of the reactor for steady-state analysis (1/8 core). FCM, fully ceramic microencapsulated.

Table 8 – Computational conditions of two-dimensional FDM in an R-Z geometry for single-channel thermal analysis.

Parameters		Values
Number of cells in axial direction		36 ($\Delta z = 10.16$ cm)
Number of cells in radial direction	Pellet	30 ($\Delta r_f = 0.01365$ cm)
	Gap	10 ($\Delta r_h = 8.5E{-}4$ cm)
	Cladding	20 ($\Delta r_c = 0.00285$ cm)
Matrix equation solver		BICGSTAB
Preconditioner		Symmetric Gauss–Seidel
Convergence criterion		1.0E–07

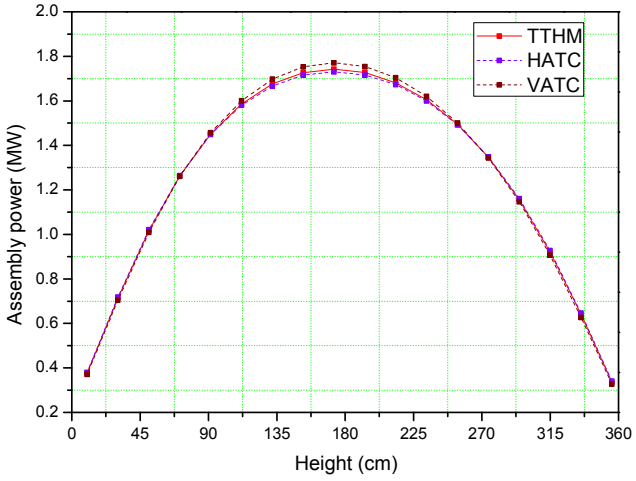

Fig. 9 – Axial power distributions of assembly (6,5). HATC, harmonic-average thermal conductivity; TTHM, two-temperature homogenized model; VATC, volumetric-average thermal conductivity.

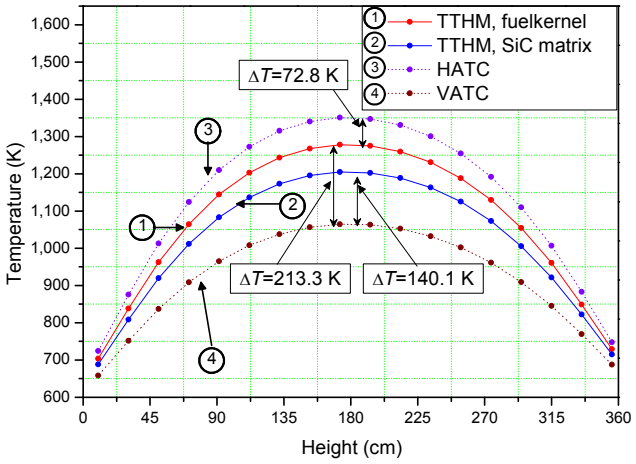

Fig. 11 – Axial temperature profiles at the centerline of the FCM fuel element in assembly (6,5). FCM, fully ceramic microencapsulated; HATC, harmonic-average thermal conductivity; SiC, silicon carbide; TTHM, two-temperature homogenized model; VATC, volumetric-average thermal conductivity.

1930.4 cm/s. The total power and maximum temperature changes during the transient state are shown in Figs. 3 and 15, respectively. The maximum power, temperatures, and average energy deposition for the first 10 seconds calculated via the models are compared in Table 11.

As shown in Fig. 15 and Table 11, the maximum total power in the two-temperature homogenized model (524.7 MW) is ~3% lower than that in the harmonic-average thermal conductivity model (542. 2 MW) and ~0.2% higher than that in the volumetric-average thermal conductivity model (523.9 MW). In addition, as shown in Table 11, the average energy deposition in the two-temperature homogenized model (346.6 J/g) is ~1% lower than that in the harmonic-average thermal conductivity model (348.7 J/g) and ~10% lower than that in the

0.3199	0.7619	1.2470	1.6100	1.7420	1.5930	1.1810	0.6199
–0.2813	–0.3938	–0.4812	–0.5590	–0.6315	–0.5650	–0.5927	–0.4839
0.3751	0.8400	1.2831	1.5528	1.6648	1.5694	1.2701	0.9840
	0.4800	0.9774	1.3690	1.5230	1.3890	0.9814	0.4740
	–0.4375	–0.4911	–0.5844	–0.5253	–0.5040	–0.4891	–0.4852
	0.8333	1.1254	1.3148	1.4445	1.3679	1.1107	0.8861
		0.5333	0.9394	1.1380	1.0380	0.6790	
		–0.4875	–0.4577	–0.4394	–0.3854	–0.4124	
		0.9563	1.0113	0.9666	0.9634	0.7953	
Power (TTHM) [MW]			0.4573	0.6791	0.6324	0.3728	
HATC-Diff[1] [%]			–0.3499	–0.2651	–0.2530	–0.2951	
VATC-Diff[2] [%]			0.7435	0.5890	0.4744	0.4024	
				0.3322	0.2828		
				–0.0903	–0.1414		
				0.0903	0.0707		

[1] $HATC\text{-diff} = \frac{HATC - TTHM}{TTHM} \times 100$

[2] $VATC\text{-diff} = \frac{VATC - TTHM}{TTHM} \times 100$

Fig. 10 – Radial power distribution at a height of z = 172.7 cm. HATC, harmonic-average thermal conductivity; TTHM, two-temperature homogenized model; VATC, volumetric-average thermal conductivity.

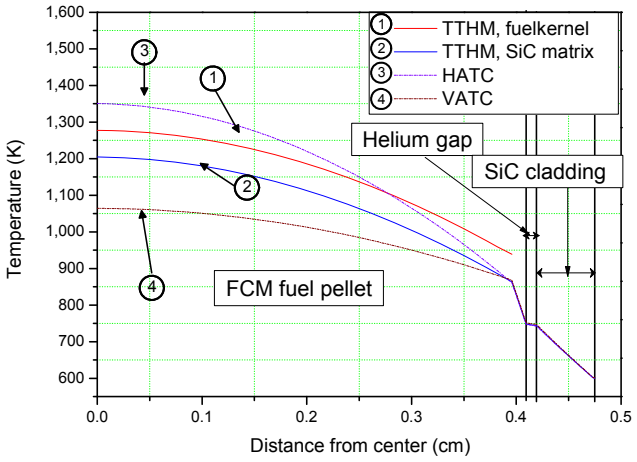

Fig. 12 – Radial temperature profiles at an elevation of z = 172.7 cm in the FCM fuel element in assembly (6,5). FCM, fully ceramic microencapsulated; HATC, harmonic-average thermal conductivity; SiC, silicon carbide; TTHM, two-temperature homogenized model; VATC, volumetric-average thermal conductivity.

volumetric-average thermal conductivity model (377.1 J/g). The causes of these results, as shown in Fig. 3, are that the fuel-kernel temperatures in the two-temperature homogenized model increase by ~32.5 K for 0.2 seconds and the Doppler temperature feedback is affected by the rapidly increased fuel-kernel temperatures. Meanwhile, in the other thermal analysis models, it is affected by the effective temperatures of the FCM pellet and these temperatures change more slowly, i.e., they increase by, at most, ~12.6 K for 0.2 seconds, since the values of the density×specific heat for the FCM pellet in the models are approximately six times higher than those of the fuel kernels in the two-temperature homogenized model. Note that in the harmonic- and volumetric-average thermal conductivity models, all constituent materials in the FCM pellet, including the fuel kernels, are assumed to be mixed homogeneously, and this is why the density × specific heat of the FCM pellet is higher.

Note that the average energy depositions from the three thermal analysis models are much lower than the regulatory limit of 628 J/g for the conventional UO_2 fuel, since the volume of fissile materials in the FCM fuel is much smaller than that in the conventional UO_2 fuel. Compared with the experimental limit of average energy deposition in the individual TRISO particle, which is 1,436 J/g [12], the average energy depositions are much lower in the three thermal analysis models.

Table 9 – Comparison of the maximum temperatures and thermal conductivities of the thermal analysis models at steady state.

	Thermal analysis models		
	TTHM	HATC	VATC
Maximum temperature (K)	1,277.8	1,350.6	1,064.5
Thermal conductivity (W/cm K) (T = 1,200 K)	0.0652 (SiC matrix)	0.0458	0.1170

HATC, harmonic-average thermal conductivity; SiC, silicon carbide; TTHM, two-temperature homogenized model; VATC, volumetric-average thermal conductivity.

Table 10 – Reactor configuration for transient-state analyses.

Parameter		Value	
		Scenario 1	Scenario 2
Power (MW) (1/8 core)		300	3
Initial control rod position (axial direction) (cm)		203.2	20.32
Speed of control rod movement (cm/sec)		1,930.4	3,860.8
Enrichment of fuel (w/o)		19.7	
Number of fuel assemblies		9	
Number of fuel rods per assembly		264	
Number of guide tubes per assembly		24	
Active length (cm)		365.8	
Guide tube	Inner diameter (cm)	1.123	
	Outer diameter (cm)	1.204	
Coolant inlet temperature (K)		555.8	

Additionally, the difference in the maximum temperatures between the two-temperature homogenized model (~1,474.3 K) and the harmonic-average thermal conductivity model (~1,551.1 K) is ~76.8 K. Meanwhile, the difference between the two-temperature homogenized model and the volumetric-average thermal conductivity model (~1,219.7 K) is ~254.6 K.

3.2.3. *Reactivity-initiated accident via fast control rod withdrawal*

In Scenario 2, initially, the control rods in assembly (6,5), in which the control rod worth is 1,079.5 pcm, are inserted at an elevation of z = 20.32 cm, as shown in Figs. 13 and 16 and Table 10, and they are withdrawn to an elevation of z = 406.08 cm with a control rod movement speed of 3,860.8 cm/s. The total power and maximum temperature changes during the transient state are shown in Figs. 17 and 18, respectively. The maximum power, temperatures, and average energy deposition calculated via the models are compared in Table 12.

As shown in Fig. 17 and Table 12, the maximum total power in the two-temperature homogenized model (6,640.7 MW) is ~2.42 times lower than those in the harmonic-average thermal conductivity model (16,061.3 MW) and volumetric-average thermal conductivity model (16,090.9 MW). In addition, the average energy deposition in the two-temperature homogenized model (393.2 J/g) is ~11% lower than that in the harmonic-average thermal conductivity model (434.9 J/g) and ~17% lower than that in the volumetric-average thermal conductivity model (461.9 J/g). The causes of these results, as shown in Fig. 18, are that the fuel-kernel temperatures in the two-temperature homogenized model increase by ~381.5 K for ~0.1 seconds and the Doppler temperature feedback is affected by the rapidly increased fuel-kernel temperatures. Meanwhile, in the other thermal analysis models, it is affected by the effective temperatures of the FCM pellets and these temperatures change more slowly, i.e., they increase by, at most, ~180 K for 0.1 seconds, since the values of the

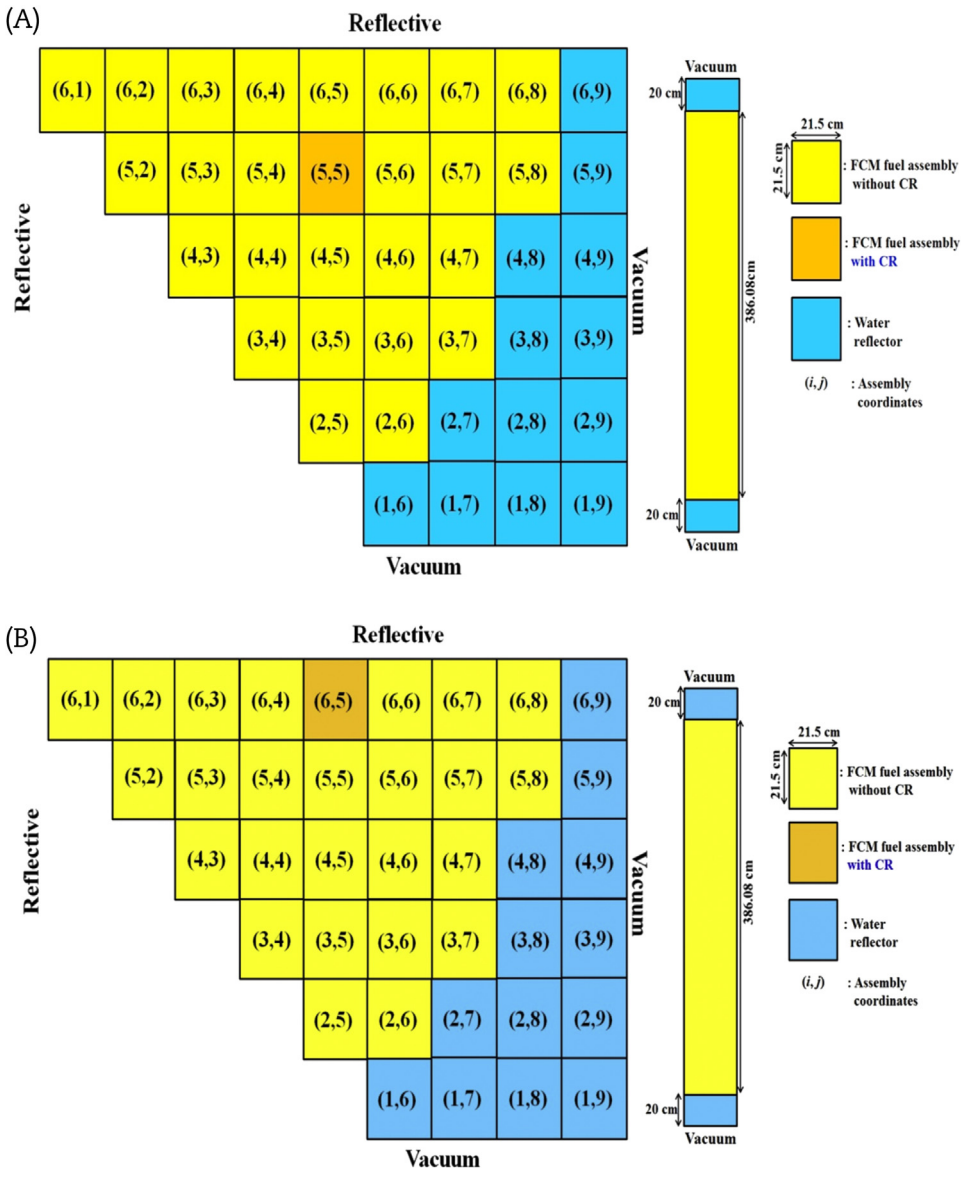

Fig. 13 – Radial and axial configuration of the reactor for transient analyses (1/8 core). (A) Reactivity-initiated accident via slow control rod withdrawal (Scenario 1). (B) Reactivity-initiated accident via fast control rod withdrawal (Scenario 2). CR, control rod; FCM, fully ceramic microencapsulated.

density × specific heat for the FCM pellet in the models are approximately six times higher than those of the fuel kernels in the two-temperature homogenized model.

The differences between the models are more pronounced than those in Scenario 1 since ~2.5 times larger reactivity (1,079.6 pcm in Scenario 2 and 432.9 pcm in Scenario 1) is inserted with approximately two times faster control rod movement speed (3,860.8 cm/s in Scenario 2 and 1,930.4 cm/s in Scenario 1). Therefore, in order to incorporate Doppler temperature feedback more realistically, especially for the scenario in which large reactivity is inserted in a short time, the fuel-kernel temperatures should be calculated explicitly.

Similarly with Scenario 1, the average energy depositions from the three analysis models are much lower than the regulatory limit of 628 J/g for the conventional UO_2 fuel, since the volume of fissile materials in the FCM fuel is much smaller than that in the conventional UO_2 fuel. Compared with the experimental limit of average energy deposition in an individual TRISO particle, which is 1,436 J/g [12], the average energy depositions are much lower for the three thermal analysis models.

Similar to the difference in the maximum power, the differences in the average energy deposition between the models are also more pronounced than those in Scenario 1. In other words, the differences in Scenario 2 are ~20%, while those in Scenario 1 are ~10%. Since ~20% differences in the average energy deposition between the models may cause significant differences in the microstructures in the TRISO particles in the FCM fuel [12], it is important to calculate the average energy deposition accurately at transient states. For an accurate calculation of the average energy deposition, Doppler temperature feedback should be performed realistically.

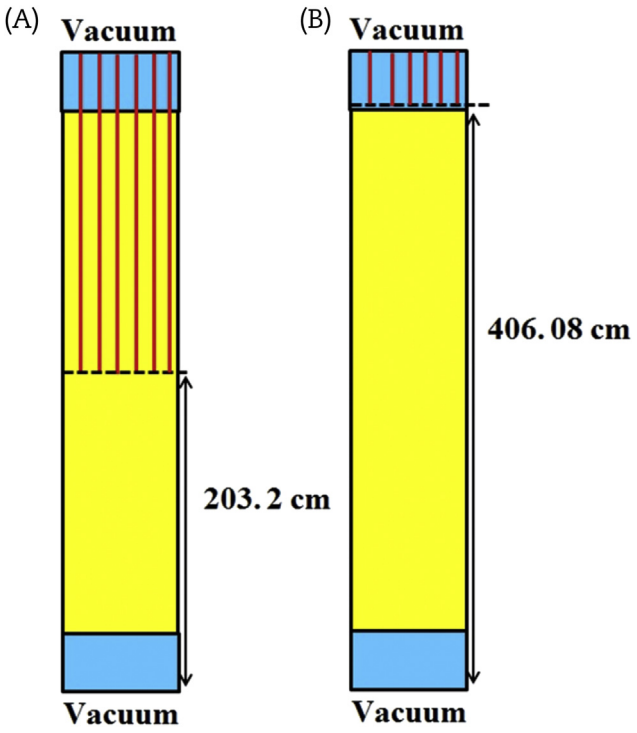

Fig. 14 – Control rod position at t = 0 seconds and t = 0.15 seconds for Scenario 1 (not in scale): (A) t = 0 seconds and (b) t = 0.15 seconds.

Additionally, the difference in the maximum temperatures between the two-temperature homogenized model (~1,059.0 K) and the harmonic-average thermal conductivity model (~1,081.7 K) is ~22.7 K. The difference between the two-temperature homogenized model and that of the volumetric-average thermal conductivity model (~977.6 K) is ~81.4 K. The differences are smaller than those at the steady state, since the scenario started with 1% of power at normal operation as the initial power.

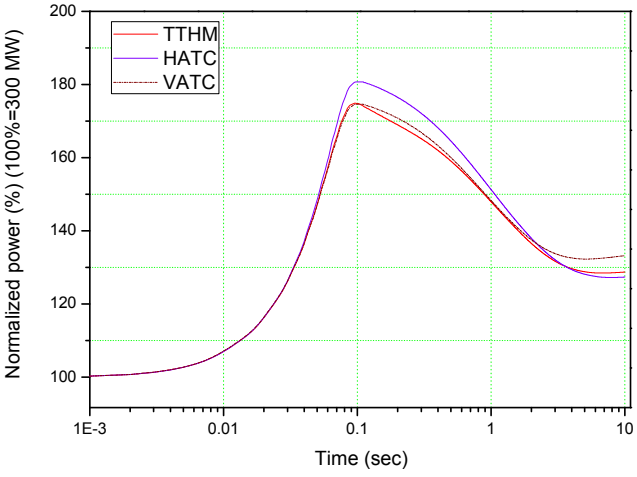

Fig. 15 – Total power changes during Scenario 1. HATC, harmonic-average thermal conductivity; TTHM, two-temperature homogenized model; VATC, volumetric-average thermal conductivity.

Table 11 – Comparison of thermal performances for the first 10 seconds during Scenario 1.

Thermal analysis models	Maximum power (MW)	Maximum temperature (K)	Average energy deposition (J/g)
TTHM Fuel kernel	524.7	1,474.3	346.6
SiC matrix		1,381.9	
HATC	542.2	1,551.1	348.7
VATC	523.9	1,219.7	377.1

HATC, harmonic-average thermal conductivity; SiC, silicon carbide; TTHM, two-temperature homogenized model; VATC, volumetric-average thermal conductivity.

4. Summary and conclusions

In this study, coupled with the COREDAX neutron diffusion model, a realistic reactor core loaded by FCM fuels, in which TRISO particles, based on a uranium nitride kernel, are randomly distributed in fine lattice stochastic structures, was analyzed via the two-temperature homogenized model at steady and transient states. The results were compared with those of the harmonic- and volumetric-average thermal conductivity models. In the analyses, thermophysical properties of the FCM pellet, including homogenized parameters in the two-temperature homogenized model and cross sections in the neutron diffusion model were considered to be temperature dependent. For the temperature feedback on the cross sections in the neutron diffusion model, the effective temperatures of the FCM fuels were calculated by preserving the reactivity from the temperature profiles.

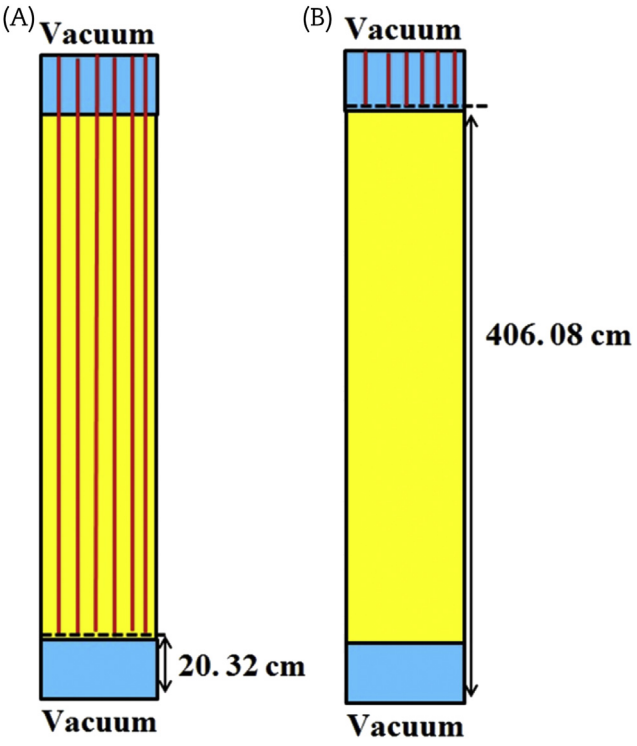

Fig. 16 – Control rod position at t = 0 seconds and t = 0.15 seconds for Scenario 2 (not in scale): (A) t = 0 seconds and (B) t = 0.15 seconds.

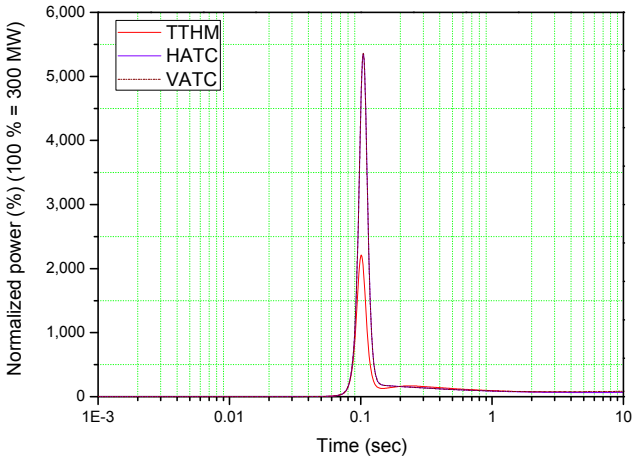

Fig. 17 – Total power changes during Scenario 2. HATC, harmonic-average thermal conductivity; TTHM, two-temperature homogenized model; VATC, volumetric-average thermal conductivity.

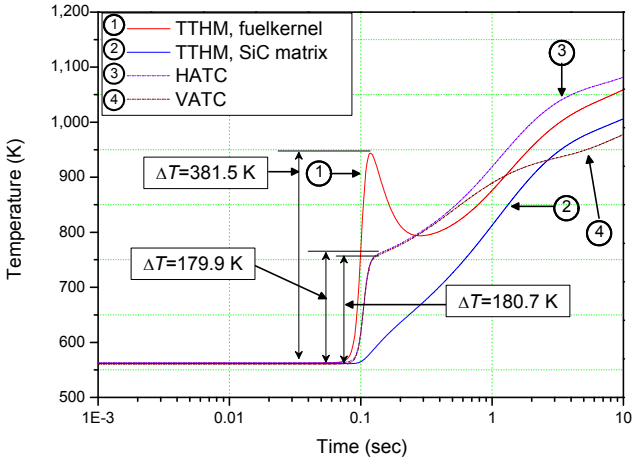

Fig. 18 – Maximum temperature changes during Scenario 2. HATC, harmonic-average thermal conductivity; SiC, silicon carbide; TTHM, two-temperature homogenized model; VATC, volumetric-average thermal conductivity.

The effective temperatures of the fuel kernels (used as the Doppler temperatures) and those of the SiC matrix, helium gap, SiC cladding, and coolant at each axial plane were considered. In the harmonic- and volumetric-average thermal conductivity models, the effective temperatures in the FCM pellet were considered as the Doppler temperatures since those models cannot provide fuel-kernel temperatures explicitly.

In the steady-state analysis, we compared the following: (1) k_{eff} eigenvalues; (2) power distributions; and (3) temperature profiles in the hottest single channel. Differences in the k_{eff} eigenvalues of the three thermal analysis models are considerable; i.e., the eigenvalues differed by ~210 pcm. There were differences of ~2% in the power distributions obtained via the thermal analysis models.

Meanwhile, the three thermal analysis models show significant differences in temperature profiles at the steady state. The maximum temperature of the two-temperature homogenized model was ~72.8 K lower than that of the harmonic-average thermal conductivity model and ~213.3 K higher than that of the volumetric-average thermal conductivity model.

In the transient-state analysis, we considered two scenarios: reactivity-initiated accident via (1) slow control rod withdrawal and (2) fast control rod withdrawal. We compared the following: (1) total power; (2) maximum temperatures in the hottest single channel; and (3) average energy deposition.

In the transient analysis, the maximum total power in the two-temperature homogenized model was ~2.42 times lower than that in the harmonic- and volumetric-average thermal conductivity models. In addition, the average energy deposition in the two-temperature homogenized model was also ~11% lower than that in the harmonic-average thermal conductivity model and ~20% lower than that in the volumetric-average thermal conductivity model. These results are attributed to the Doppler temperature feedback being affected by the fuel-kernel temperatures that are calculated explicitly. Since ~20% differences in the average energy deposition between the models may cause significant differences in the microstructures in the TRISO particles in the FCM fuel, it is important to calculate the average energy deposition accurately at transient states. For an accurate calculation of the average energy deposition, Doppler temperature feedback should be performed realistically.

The three thermal analysis models also show significant differences in temperature profiles in the transient-state analysis. In the scenario involving a reactivity-initiated accident via slow control rod withdrawal, the maximum temperature of the two-temperature homogenized model was ~76.8 K lower than that of the harmonic-average thermal conductivity model and ~254.6 K higher than that of the volumetric-average thermal conductivity model.

Table 12 – Comparison of thermal performances for the first 4 seconds during Scenario 2.

Thermal analysis models		Maximum power (MW)	Maximum temperature (K)	Average energy deposition (J/g)
TTHM	Fuel kernel	6,640.7	1,059.0	393.2
	SiC matrix		1,006.2	
HATC		16,061.3	1,081.7	434.9
VATC		16,090.9	977.6	461.9

HATC, harmonic-average thermal conductivity; SiC, silicon carbide; TTHM, two-temperature homogenized model; VATC, volumetric-average thermal conductivity.

In summary, for a thermal analysis of FCM fuel, the two-temperature homogenized model can provide more realistic temperature profiles than the harmonic- and volumetric-average thermal conductivity models. Moreover, the presented model can distinguish between the fuel-kernel temperature and the SiC matrix temperature. Such aspects of the two-temperature homogenized model enable it to perform Doppler temperature feedback more realistically than the other models, particularly in scenarios in which power changes very rapidly.

In addition, the two-temperature homogenized model can be applied to other geometrical types of fuels in which coated particles are randomly dispersed, such as pebble bed and prismatic block-type VHTRs [13], coated particle-dispersed plate fuel loaded in a novel research reactor [14], and FCM fuel in a CANDU reactor [15].

Conflict of interest

No conflict of interest.

REFERENCES

[1] Y. Lee, B. Cho, N.Z. Cho, Steady- and transient-state analyses of fully ceramic microencapsulated fuel with randomly dispersed TRISO particles via two-temperature homogenized model—I: theory and method, Nucl. Eng. Technol. 48 (2016) 650–659.
[2] H. Yu, N.Z. Cho, Comparison of Monte Carlo simulation models for randomly distributed particle fuels in VHTR Fuel Element, Trans. Am. Nucl. Soc. 95 (2006) 719–721.
[3] B. Cho, N.Z. Cho, Y. Kim, Theory Manual for the Rectangular Three-Dimensional Diffusion Nodal Code COREDAX-2 Version 1.5, KINS/HR-1356 Rev. 1, NURAPT-2015-02, Korea Advanced Institute of Science and Technology/Korea Institute of Nuclear Safety, 2015.
[4] S.B. Ross, M.S. El-Genk, Thermal conductivity correlation for uranium nitride fuel between 10 and 1923 K, J. Nucl. Mater. 151 (1988) 313–317.
[5] IAEA, Thermophysical Properties Database of Materials for Light Water Reactor and Heavy Water Reactors, IAEA-TECDOC-1496, Vienna (Austria), 2006.
[6] L.L. Snead, T. Nozawa, Y. Katoh, T.-S. Byun, S. Kondo, D.A. Petti, Handbook of SiC properties for fuel performance modeling, J. Nucl. Mater. 371 (2007) 329–377.
[7] K.A. Terrani, J.O. Kiggans, C.M. Silva, C. Shih, Y. Katoh, L.L. Snead, Progress on matrix SiC processing and properties for fully ceramic microencapsulated fuel form, J. Nucl. Mater. 457 (2015) 9–17.
[8] J. Leppänen, M. Pusa, T. Viitanen, V. Valtavirta, T. Kaltiaisenaho, The Serpent Monte Carlo code: status, development and application in 2013, Ann. Nucl. Energy 82 (2015) 142–150.
[9] R.E. MacFarlane, D.W. Muir, R.M. Boicourt, A.C. Kahler, The NJOY Nuclear Data Processing System, Version 2012, LA-UR-12-27079, Los Alamos National Laboratory, 2012.
[10] J.J. Duderstadt, L.J. Hamilton, Nuclear Reactor Analysis, John Wiley & Sons Inc., New York, 1975.
[11] J.D. Stempien, Behavior of Triplex Silicon Carbide Fuel Cladding Designs Tested under Simulated PWR Conditions, MS Thesis, MIT, Cambridge (MA), 2011.
[12] M. Umeda, T. Sugiyama, F. Nagase, T. Fuketa, S. Ueta, K. Sawa, Behavior of coated fuel particle of high-temperature gas-cooled reactor under reactivity-initiated accident conditions, J. Nucl. Sci. Technol. 47 (2010) 991–997.
[13] A.C. Kadak, R.G. Ballinger, M.J. Driscoll, S. Yip, D.G. Wilson, H.C. No, J. Wang, H. MacLean, T. Galen, C. Wang, J. Lebenhaft, T. Zhai, D.A. Petti, W.K. Terry, H.D. Gougar, A.M. Ougouag, C.H. Oh, R.L. Moore, G.K. Miller, J.T. Maki, G.R. Smolik, D.J. Varacalle, Modular Pebble Bed Reactor Project: University Research Consortium Annual Report, INEEL/EXT-2000–01034, Idaho National Engineering & Environmental Laboratory, 2000.
[14] R. Hidayatullah, D. Hartanto, Y. Kim, A novel research reactor concept based on coated particle,, Ann. Nucl. Energy 77 (2015) 477–486.
[15] D. Hartanto, Y. Kim, F. Venneri, Neutronics evaluation of a super-deep-burn with TRU fully ceramic microencapsulated (FCM) fuel in CANDU, Prog. Nucl. Energy 83 (2015) 261–269.